Urban Climate 24 (2018) 80–93 https://doi.org/10.1016/j.uclim.2018.02.002

Pollutant fluxes in two-dimensional street canyons

Annalisa Di Bernardino[1], Paolo Monti[1], Giovanni Leuzzi[1], Giorgio Querzoli[2]

[1] DICEA, Università di Roma "La Sapienza", Via Eudossiana 18, 00184 Roma, Italy.
[2] DICAAR, Università degli Studi di Cagliari, Via Marengo 2, 09123 Cagliari, Italy.

Highlights

- A line source is used to simulate vehicular emission at street level
- Velocity and tracer concentration are measured simultaneously
- Momentum and concentration fluxes are analyzed
- Venting and re-entrainment mechanisms are quantified

Abstract

The turbulent dispersion of a passive tracer emitted by a line source simulating vehicular traffic in an idealized urban canyon in neutral conditions is studied in the water channel by means of simultaneous measurements of velocity and concentration fields. The experiments are conducted for two geometrical arrangements of two-dimensional obstacles reproducing the skimming flow (AR=1) and the wake-interference regime (AR=2), where AR is the canyon aspect ratio. The results show a strict connection between the dynamics of the shear layer developing at the top of the canyon and the vorticity field. For AR=1, it is found that the shear layer flaps upwards and downwards according to two different frequencies. The greatest of them matches the vortex shedding frequency as measured at the canyon top, while the lower is comparable to H/u_* (H is the building height and u_* a reference friction velocity). The shear layer flapping modulates in time the pollutant exchange rate between the canyon and the outer layer. The different characteristics of the shear layer found for the two flow regimes also explain the larger pollutant re-entrainment observed for AR=1, which turns out to be greater than the emission rate at the source. Sweep and ejection modes are identified via quadrant analysis and used to quantify the weights of the factors involved in the turbulent exchanges of tracer and momentum between the canyon and the outer layer. It is found that the venting of polluted fluid at the canyon top increases substantially passing from AR=1 to 2, while an opposite trend is observed for the entrainment of polluted fluid. The vertical flux of pollutant at the canyon top for AR=2 is largely of turbulent nature, with the contribution of the mean flux being practically negligible. On the other hand, the latter becomes comparable or even exceeds the magnitude of the turbulent flux when AR=1. The maps of the first three statistical moments of the pollutant concentration for the two geometrical arrangements are also reported and discussed.

Keywords: Urban canyon; Street source; Concentration variance; Concentration flux; Feature tracking; Water channel.

1. Introduction

The complex building arrangements, the extremely variable locations of the pollutant sources as well as the incomplete knowledge of the turbulence processes characterizing urban canopy flows make the investigation of flow and dispersion of contaminants in urban canopies a very difficult task (Fernando, 2010; Barlow, 2014; Buccolieri et al., 2015).

Numerous studies have shown the importance of the building geometry on the microscale turbulence and the way the latter strongly affects pollutant dispersion (e.g. Liu et al., 2004). Among the infinite set of building geometries found in real cities, the two-dimensional street canyon can be considered as a basic morphological unit of the urban texture. It is defined as the space above a narrow street edged by series of parallel, tall buildings. Hussain and Lee (1980) showed that for this kind of geometrical configuration the flow can be classified based on the canyon aspect ratio, AR=W/H, where W and H are the spacing between two adjacent buildings and their average height, respectively. Under isothermal conditions, Oke (1987) identified the skimming flow (AR$\lesssim$1.5), where a single vortex forms within the cavity, the wake-interference regime (1.5$\lesssim$AR$\lesssim$2.5), in which two counter-rotating vortices develop in the street canyon, and the isolated roughness regime (AR$\gtrsim$2.5), where the interaction between individual buildings is weak or absent.

In the case of the skimming flow or wake-interference regime and wind blowing perpendicularly to the street axis, the flow within the canyon separates from that above it. This causes poor canyon ventilation, even when the external winds are strong, and pollutant stagnation. As a result, pollutants emitted by vehicular traffic at street level remain trapped within the cavity, causing high concentrations at pedestrian level. This separation is one of the main causes of air quality deterioration in cities and is partially governed by the shear layer at the canyon top, which plays a key role in the exchange of air and scalars between the canopy and the overlying region. The shear layer forms because of the large velocity gradients occurring at the canopy top. These give rise to Kelvin-Helmholtz type instabilities, which govern mass, energy and momentum exchange rates between the inner and the outer flow. Louka et al. (2000) conjectured that such instabilities cause the vertical flapping of the shear layer that, in turn, regulates the intrusion of fresh fluid from the outer layer into the canyon and, vice-versa, expulsion of pollutants from the canyon into the outer flow (see also Takimoto et al., 2011). Salizzoni et al. (2009a, 2011) showed by means of wind-tunnel measurements how the shear layer dynamics are influenced by turbulent kinetic energy fluxes from the external flow which, in turn, depends on the oncoming boundary layer.

Analysis on pollutant fluxes had come mainly from large eddy simulations (LES). For example, Liu et al. (2005) investigated fluxes of scalars emitted by a line source placed at the bottom of the canyon for different AR values. They found that the amount of pollutants trapped within the canyon

increases as AR decreases, particularly at ground level. Besides, they showed that gradient diffusion models are intrinsically unable to predict pollutant dispersion with reasonable accuracy. More recently, Li et al. (2010, 2016) investigated the effects on flow and pollutant transport of the stratification for a two-dimensional array of obstacles with AR=1, while O'Neill et al. (2016) analyzed both the statistical moments of the pollutant concentration and the vertical component of the turbulent pollutant flux, focusing on their trends at the canyon top.

Owing to intrinsic problems related to the employment of intrusive sensors, only few investigators studied pollutant fluxes in canopy flows experimentally. The main difficulty is to measure simultaneously velocity and scalar concentration fields with high spatial and temporal resolution as well. Therefore, most of the studies that have been reported so far essentially concern measurements conducted in few points of the domain (Kastner-Klein and Plate, 1999; Barlow et al., 2004). In recent years, the use of image analysis techniques has permitted the determination of turbulent fluxes of scalars in the water channel or in the wind tunnel (see e.g. Vinçont et al., 2000; Dezső-Weidinger et al., 2003; Monti et al., 2007; Tomas et al., 2017). Nevertheless, several aspects of the flow structure are still unknown and need to be clarified in order to improve knowledge about pollutant dispersion in urban environments. For example, it would certainly be of interest to know how pollutant and momentum fluxes at the canyon top depend on the canyon aspect ratio.

In this work, we aim to analyze the dispersion mechanisms of a passive pollutant discharged into a two-dimensional urban canyon – reproduced in a water-channel facility – by measuring simultaneously velocity and scalar concentration fields with high temporal and spatial resolutions. Both the skimming flow and wake-interference regimes are analyzed and particular attention is paid to turbulent momentum and scalar fluxes within the cavity, especially at the shear layer.

The paper is organized as follows. Section 2 gives a description of the laboratory facility and the acquisition technique, while Section 3 presents the results obtained for the two geometries investigated. Both the spatial distribution of the first three statistical moments of the tracer concentration and the maps of the vertical momentum and tracer fluxes are presented, focusing on their trends calculated at the canyon top. Finally, the Pollutant Exchange Rate (PCH) and the Air Exchange Rate (ACH), two useful parameters introduced by Liu et al. (2005), are also determined and discussed. In Section 4, the most important conclusions of the work are summarized.

2. Experimental setup and measurement technique

The experiments are performed in a recirculating water channel located at the Hydraulic Laboratory of the University of Rome – La Sapienza. This water channel has a rectangular cross section of 0.35m height and 0.25 m width and a length of 7.40 m. To observe the flow visually, the

lateral sides of the tank are made of transparent glass. A constant head reservoir feeds the flume and a floodgate, located at the end of the channel, regulates the water depth and, therefore, the water velocity. Three honeycombs are positioned at the opening section of the channel to minimize unwanted effects due to the inlet system. To recreate the naturally grown atmospheric boundary layer in the water channel, the roughness of the channel bottom is increased by means of randomly distributed pebbles (average diameter ≈5 mm), glued onto the bottom (Figure 1). Downstream of the pebbles, a series of evenly spaced parallelepipeds with square section B=H=20 mm (here B indicates the building width) and length equal to the channel width are glued onto the channel bottom, normally to the streamwise velocity (for further details on the experimental setup see Di Bernardino et al., 2015a).

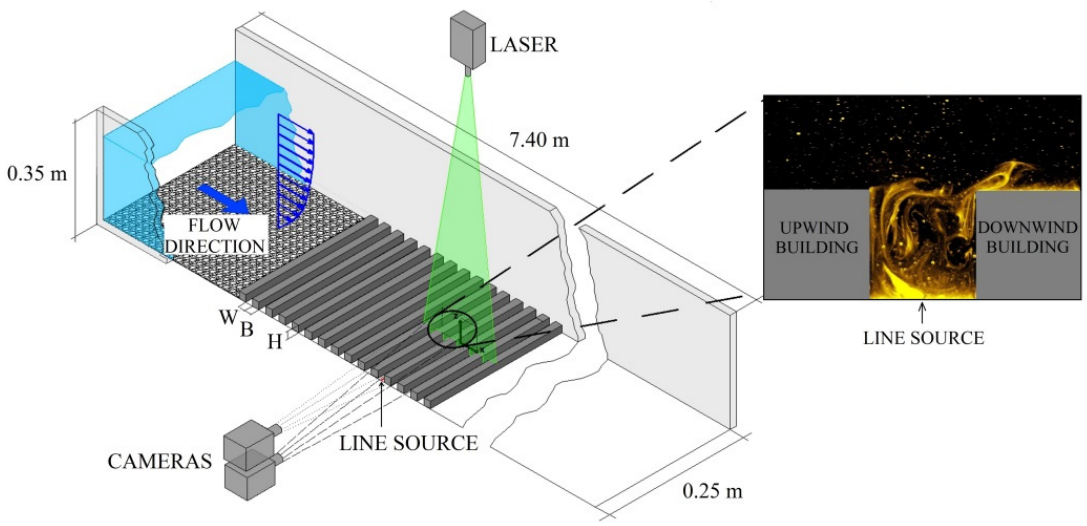

Fig. 1. Sketch of the laboratory facility. The enlargement shows a non-filtered snapshot (AR=1).

Two geometrical configurations are investigated by varying the distance (W) between the obstacles. In particular, the skimming flow and the wake-interference regime are simulated by setting W=20 and 40 mm to obtain street canyons with AR=1 and 2, respectively. The test section is located nearly 5 m downstream of the inlet, where the boundary layer is fully developed and the water depth is 0.16 m. The Reynolds number of the flow, $Re = UH/\nu$, based on the free stream velocity, U=0.33 m s^{-1}, is nearly 50000 ($\nu=10^{-6}$ m^2s^{-1} is the kinematic viscosity of water), while the roughness Reynolds number, $Re_* = u_*H/\nu$, is 380 for AR=1 ($u_*\approx0.019$ m s^{-1} measured within the constant flux layer) and 540 for AR=2 ($u_*\approx0.027$ m s^{-1}). Therefore, both the simulated large-scale structures and the mean flow can be considered as being independent of Re (fully rough wall regime, see Snyder (1972); Uehara et al. (2003). For additional information on the Re independence of the flow simulated in the present water channel see Di Bernardino et al., 2015b).

Ground-level pollutant emission due to vehicular traffic is simulated by means of a line source consisting of a 1 mm wide slot placed at the center of the bottom of the cavity and parallel to its longitudinal axis (Figure 1). A continuous emission of a mixture of Rhodamine-WT and water is delivered to the source by gravity (concentration at the source: $c_0=8\cdot10^{-4}$ g l^{-1}). Rhodamine-WT is a passive (chemically inert and neutrally buoyant) fluorescent dye that, excited by a green light (532 nm) emits red light (587 nm). The mixture reaches the source through a thin pipe, connected to a constant head reservoir that guarantees a constant rate discharge. The velocity of the mixture through the slot is under 0.5 cm s^{-1}, i.e. well below the fluid velocity within the cavity. Consequently, the momentum of the scalar jet at the source is considerably smaller compared to that of the local main flow, ensuring the absence of a significant mechanical rise of the polluted plume within the canyon.

The streamwise (u) and vertical (w) velocity components and the tracer concentration (c) are measured simultaneously on a vertical section passing through the longitudinal axis of the channel. The acquisition facility consists of a green laser (5 W, wavelength 532 nm) emitting a thin light sheet (2 mm thick) illuminating the acquisition plane and two synchronized cameras (1024x1280 pixels in resolution) acquiring 250 frames per second. The framed area is 93 mm wide (x-axis) and 74 mm high (z-axis). The two cameras are aligned vertically to optimize the framing of the area of interest (i.e. the canyon and the downstream building) and to reduce image distortion as much as possible.

The first camera acquires the positions of the non-buoyant particles (20 μm in diameter) immersed in the fluid and allows the evaluation of the instantaneous velocity fields by means of a feature-tracking algorithm based on image analysis (Cenedese et al., 2005). A Gaussian interpolation algorithm is applied for each time instant to the scattered samples on the x-z plane to obtain the instantaneous velocity field on a regular 186x148 array, which corresponds to a 0.5 mm spatial resolution (i.e. H/40). To sense only the fluorescent light emission, the second camera is equipped with a narrow band pass filter tuned on 587 nm. The concentration measurements are achieved via planar laser-induced fluorescence (PLIF), a technique typically employed for the investigation of tracer dispersion in water channels (Pournazeri et al., 2013). Images are calibrated so that the Rhodamine-WT concentration at a given pixel (directly related to the fractional volume of the dyed fluid) is proportional to the luminosity measured. To permit the investigation of the scalar flux, the instantaneous concentration field is mapped onto the velocity field using an affine transformation that maps the velocity field on the concentration field accounting for the different points of view of the two cameras (see Monti et al. 2007 for details on this procedure). In this

process, the superimposition of the velocity and concentration fields is obtained by assigning to each grid cell the value of the concentration at the center of the cell.

25,000 instantaneous velocity and concentration fields have been measured during the experiments, corresponding to a 100 s long acquisition time. By assuming $T = H/u_*$ as the time scale of the flow (nearly 1 s, i.e. the time needed by a fluid particle to travel a complete recirculation within the canyon), the duration of the experiments is long enough to assure that the analysis is robust from a statistical point of view. By applying the canonical Reynolds averaging method, the mean velocity components, $\bar{u}$ and $\bar{w}$, the variances $\overline{u'^2}$ and $\overline{w'^2}$ as well as the vertical momentum flux $\overline{u'w'}$ are calculated in each node of the 186x148 grid. Here, the bar indicates the time average, while the prime is the fluctuation around the mean. Similarly, the mean, $\bar{c}$, the standard deviation, $\sigma_C = \sqrt{\overline{c'^2}}$, and the skewness factor, $S_C = \overline{c'^3}/(\sigma_C)^3$, of the Rhodamine-WT concentration were determined on the 1024x1280 array of the image pixels.

3. Results

3.1. Initial description

Before discussing the details of the data collected during the experiments, it is useful to recall the main differences between skimming flow and wake-interference regimes. Details on two-dimensional canopy flows based on the same experimental setup used in the present work can be found in Di Bernardino et al. (2015a) and (2017). These authors reported information on the approaching flow and on the two-dimensional fields of average velocity, variance, skewness factor as well as various terms involved in the balance equation of the turbulent kinetic energy for four aspect ratios, ranging from 1 to 2. Interesting insights into two-dimensional canopy flows based on laboratory studies have been given by Baik et al. (2000), Baik and Kim (2002), Caton et al. (2003), Barlow et al. (2004), Salizzoni et al. (2011) and Neophytou et al. (2014), among others.

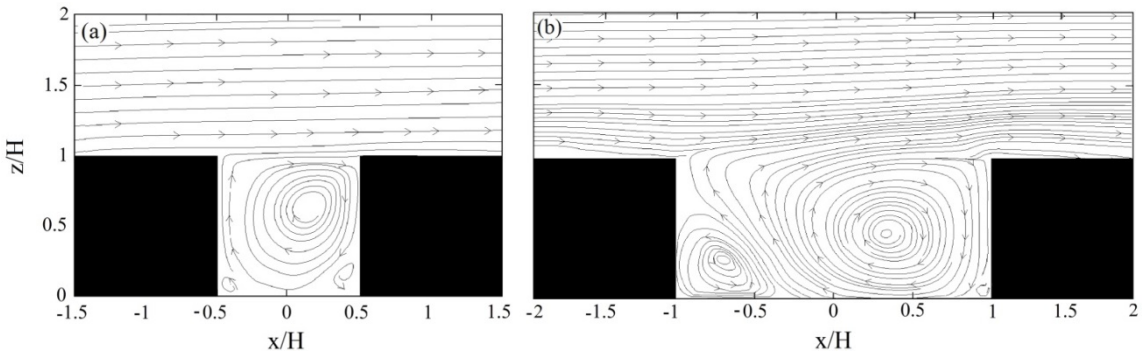

Fig. 2. Streamlines determined from the mean velocity field for (a) AR=1 and (b) AR=2.

Figures 2a and b depict the streamlines of the mean velocity fields measured for AR=1 and 2, respectively. Note that the streamlines have been obtained in the presence of the source at the cavity bottom; therefore, some of them flow out of the top of the canyon for continuity constraint. For AR=1, the flow shows the typical features of the skimming flow, i.e. a main vortex (rotating clockwise) governing the flow within the canyon and a current nearly parallel to the streamwise direction (from left to right) in the overlying boundary layer. Two small, counter-rotating vortices form at the bottom corners of the canyon. For AR=2, a second (anti-clockwise) vortex occupies a large portion of the upstream side of the canyon, in line with the flow topology characterizing the wake-interference regime.

It is worthwhile to note that previous studies regarding 2D canopy flows for AR=2 showed a well-developed counter-rotating vortex, as in the numerical simulations by Kovar-Panskus et al. (2002) and Liu et al. (2004) as well as in the laboratory experiments by Brevis et al. (2014) and Garau et al. (2018). On the other hand, the experiment made by Neophytou et al. (2014) for an aspect ratio of nearly 2 does not show a well-defined counter-rotating vortex in the upwind facet of the canyon. The reason of those disparities is not clear. Liu et al. (2004) argued that an inadequate spatial resolution could explain the difficulty of numerical models in producing the secondary circulations, even though recent numerical simulations by Brevis et al. (2014) seem to contradict the previous hypothesis. One possible explanation might be the different nature of the external flow. In fact, the characteristics of the approaching boundary layer have a significant influence on the turbulent exchange of mass and momentum at the top of the canyon and, therefore, on the flow within the cavity (Salizzoni et al. 2009a, 2009b, 2011). As shown below, the different flow topology is one of the main reasons for the large differences observed for the concentration fields for the two AR values.

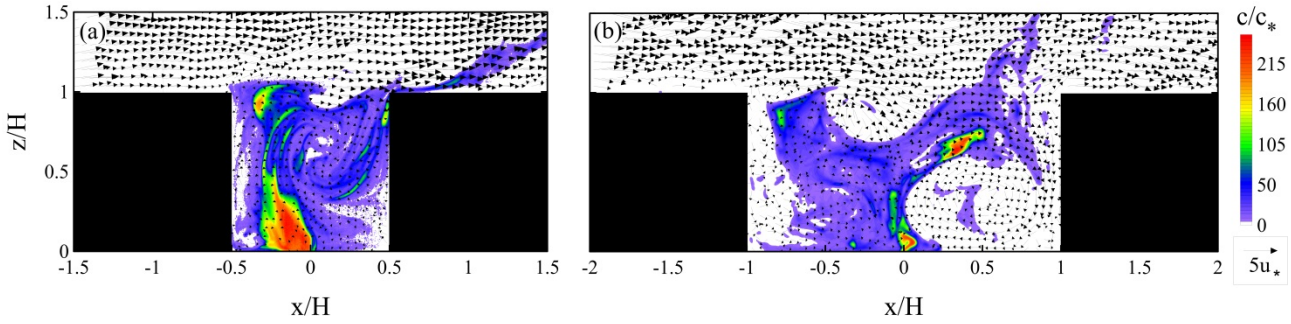

Fig. 3. Instantaneous velocity (vectors) and concentration (colors) fields for (a) AR=1 and (b) AR=2.

Additional basic differences between the two regimes can be discerned by comparing instantaneous velocity (vectors) and concentration (colors) fields. In what follows, the tracer

concentration is normalized by the reference concentration, $c_* = q/u_*\Omega$, where q=Q/L is the mass rate for unit length of the source and $\Omega=(H\cdot W)^{0.5}$ is a length scale based on the canyon size. Figures 3a and b show two snapshots taken for AR=1 and 2, respectively. In the former case, high-concentration blobs propagating from the source are advected upward by the main vortex governing the flow. A sharp concentration interface at the canyon top separates the inner (polluted) fluid from the outer (fresh) fluid. Kelvin-Helmholtz instabilities triggered by high velocity gradients enhance vertical mixing of mass and momentum at the interface. For AR=2 the pollutant is carried by the secondary vortex and spreads out quickly within the upstream side of the cavity. A second branch of the plume is carried by the right-hand side vortex. Fresh fluid enters into the canyon mainly through the right-hand part of the canyon top and makes the downstream side of the cavity practically free of pollutants.

Figure 4 shows some of the longest particle trajectories tracked during the two experiments. They all pass through the red square located at the trailing edge of the upstream building, without investigating where they came from originally. For AR=1 (Figure 4a), most of the particles move streamwise, remain lumped and pass above the windward building. Only a small number of them enters into the cavity (≈17% of the 200 depicted in the figure). In contrast, the particles show rather irregular paths when AR=2 (Figure 4b). Some of them pass well above the top of the windward building, while the remainder enters into the canyon (≈30%). Apparently, the salient mechanism is simply the existence of two preferred particle paths. As will be shown below, the two paths can be interpreted as signatures of the shear layer flapping, which causes upward and downward flows around the canyon top and consequent exchange of fluid between the cavity and the outer region. Clearly, one should bear in mind in interpreting the results that the approaching boundary layers are different for the two cases.

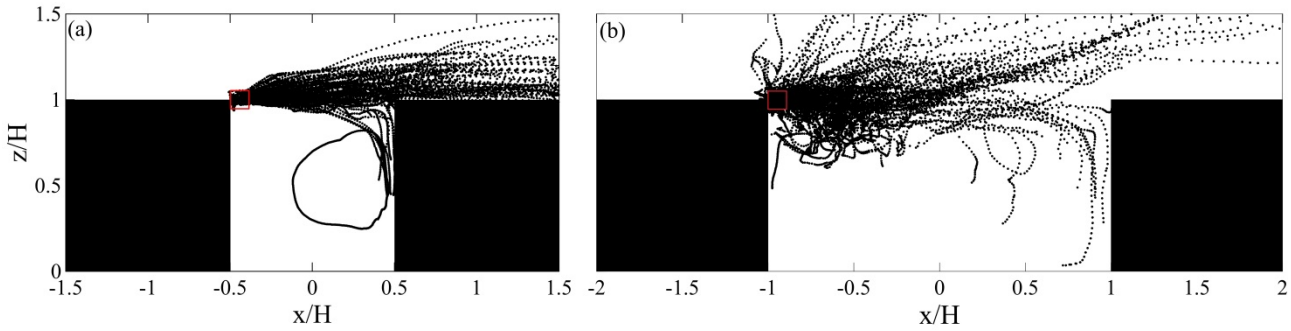

Fig. 4. Particle trajectories passing through the area delimited by red square for (a) AR=1 and (b) AR=2.

3.2. Shear layer dynamics

As outlined by Takimoto et al. (2011) in their study of flow and turbulence over a regular array of cubic obstacles, the vorticity field can be used to identify the shear layer position as the latter roughly corresponds with the region of high vorticity (ω) around the cavity top. In what follows, $\omega = (\partial u/\partial z - \partial w/\partial x)/2$ will be non-dimensionalized as ωT. For AR=1 the vortex sheet is on average horizontal and lying above the roof level (Figure 5a). In contrast, for AR=2 the vortex sheet shows lower vorticity values everywhere, is smeared out and, especially, bent downwards (see Figure 5b and the snapshot in Figure 3b).

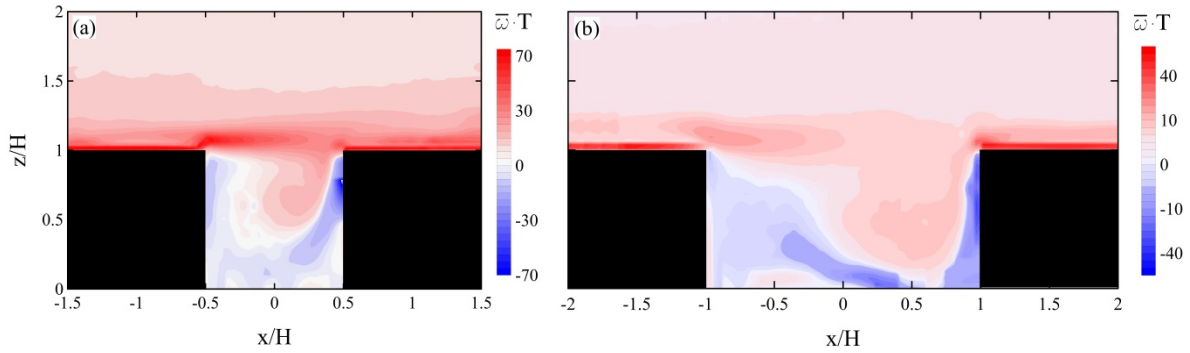

Fig. 5. Average non-dimensional vorticity fields for (a) AR=1 and (b) AR=2.

The instantaneous vorticity field in Figure 6a (colors) corresponds to an event of flushing observed for AR=1, i.e. the upward motion that causes expulsion of fluid from the canyon into the outer layer (see the inset in the figure). Conversely, events of downflow are accompanied by the intrusion into the canyon of clean fluid from above and by a tongue of high vorticity near the windward building (Figure 6b). Louka et al. (2000) conjectured that the vertical flapping of the shear layer is caused by Kelvin-Helmholtz type instabilities that, in turn, regulates the intrusion of fresh fluid from the outer layer into the canyon and, vice-versa, the expulsion of pollutants from the canyon into the outer flow (see also Takimoto et al., (2011)). As mentioned above, the dynamics of the shear layer at the top of the canyon are influenced by the turbulent kinetic energy flux from the external flow (see Salizzoni et al. (2011) and reference cited therein).

Careful inspection of the data reveals that the upward and downward motion of the shear layer follows a well-defined dynamics. The normalized power spectral density of w-velocity calculated in one point of the region occupied on average by the shear layer (x/H=-0.25; z=H) shows a dominant frequency at nearly 2.3 Hz (Figure 7a). That value is quite close to the Strouhal frequency of the flow, $f_s = SU/L$=2.35 Hz (here S is the Strouhal number and L a characteristic length), as f_s is calculated assuming L as the canyon diagonal and S=0.2, as the latter commonly associated to vortex-shedding behind bluff bodies (see e.g. Dutta et al. (2003) and Zajic et al. (2003)) or in

canopy flows (Poggi et al. 2008). The time period (≈1 s) corresponding to the second distinct peak at ≈1 Hz is nearly T, i.e. the time scale related to the recirculation time within the canyon (see Sect. 2). That the intermittent behavior of the shear layer bears relation to the vortex shedding can be further corroborated simply upon inspection of the normalized power spectral density of the Pollutant Exchange Rate (PCH) shown in Figure 7b (see Sect. 3.4 for the definition of PCH). It is apparent that the frequencies of the two highest peaks compare well with those observed in Fig. 7a, suggesting that a strong relation between concentration fluxes at the canyon top and shear layer flapping holds. More discussion on this issue is given in Sects. 3.3 and 3.4.

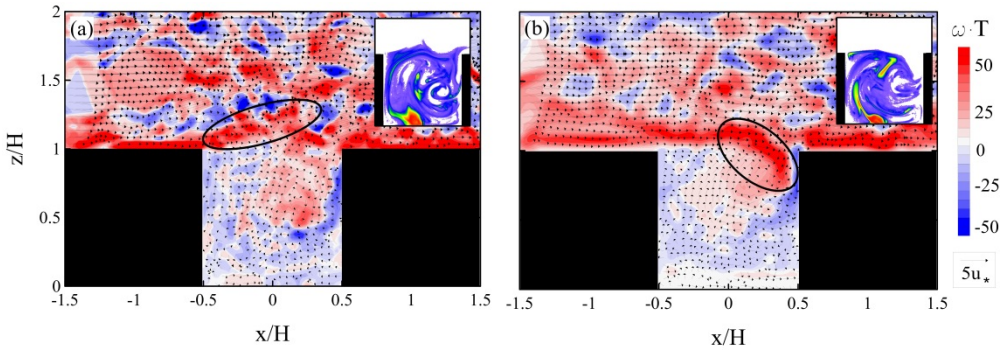

Fig. 6. Instantaneous snapshots showing contours of non-dimensional vorticity, ωT, and vector maps of the velocity field for AR=1. (a) Upward shear layer, (b) downward shear layer. The black ellipses indicate the positions of the shear layer. The two insets depict the corresponding (instantaneous) concentration fields.

For AR=2, the instantaneous vortex sheets are not as well-structured as for the skimming flow, particularly when the shear layer moves upward. Nevertheless, updraft of polluted fluid from the cavity is still noticeable (Figure 8a). On the other hand, events of downward bending are easily observable (Figure 8b). It is worthwhile noting that the vortex sheet never extends to the windward building but covers at the most half the canyon top.

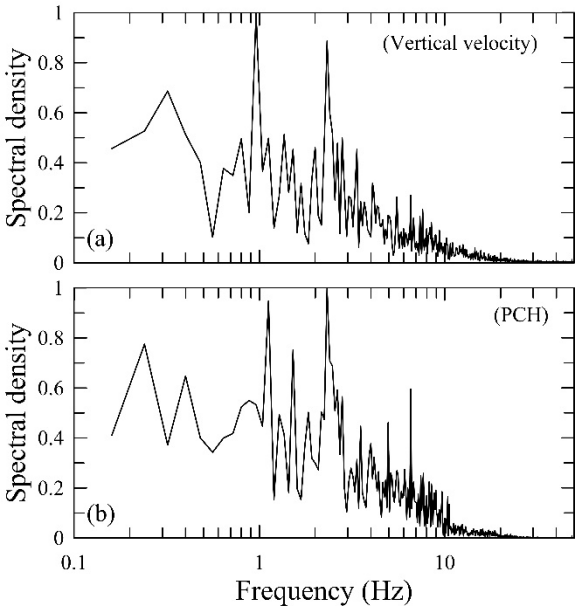

Fig. 7. Normalized power spectra of vertical velocity (a) and PCH (b) calculated at (x/H=-0.25; z=H).

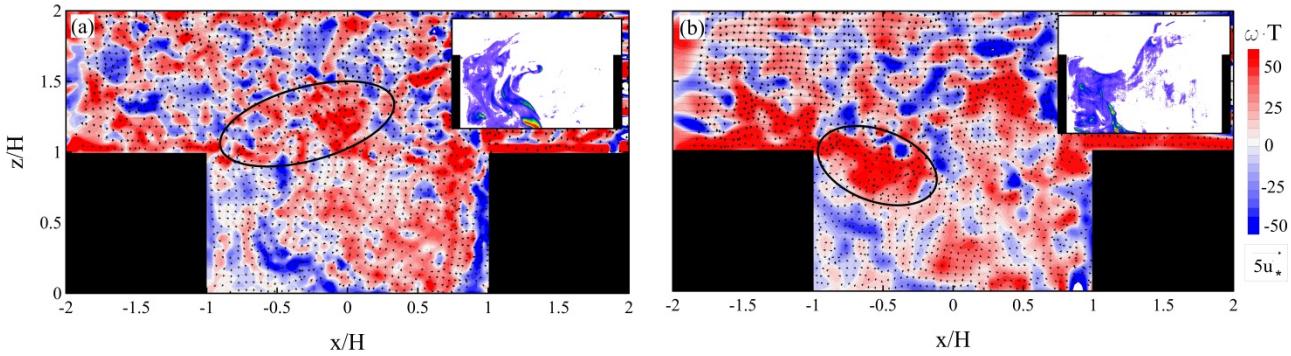

Fig. 8. As in Fig. 6, but for AR=2.

According to the procedure followed by Takimoto et al. (2011) we look for possible links between the vortex sheet location and the so-called sweep ($u' > 0$, $w' < 0$) and ejection ($u' < 0$ and $w' > 0$) events at the canyon top (Krogstad et al. (2005)). Although the instantaneous flux $u'w'$ is negative in both the events (and generally predominant in that the average vertical momentum flux, $\overline{u'w'}$, is negative at z=H), sweeps are related to entrainment of higher-speed fluid within the canyon, while ejections are linked to expulsion of lower-speed fluid from the canyon. The non-dimensional vorticity fields calculated during those two events, identified on the basis of the signs of the fluctuating velocity components measured at (x=0, z=H), have been averaged and the corresponding maps are shown in Figures 9 (AR=1) and 10 (AR=2). Downward and upward bending of the vortex sheet correlates reasonably well with sweeps (Figures 9a and 10a) and ejections (Figures 9b and 10b), even though definite conclusions are not possible for the latter case when AR=2 because of the difficulty of distinguishing the area of vorticity maxima (similar

problems were encountered by Takimoto et al., 2011). However, irrespective of the aspect ratio, sweep events exhibit higher positive vorticity at the shear layer, and lower negative vorticity regions within the canyon, compared to ejection events. Note that the maps in Figures 9 and 10 do not change appreciably if the reference point used to identify sweeps and ejections is moved from (x=0, z=H) along the canyon top or upward as well.

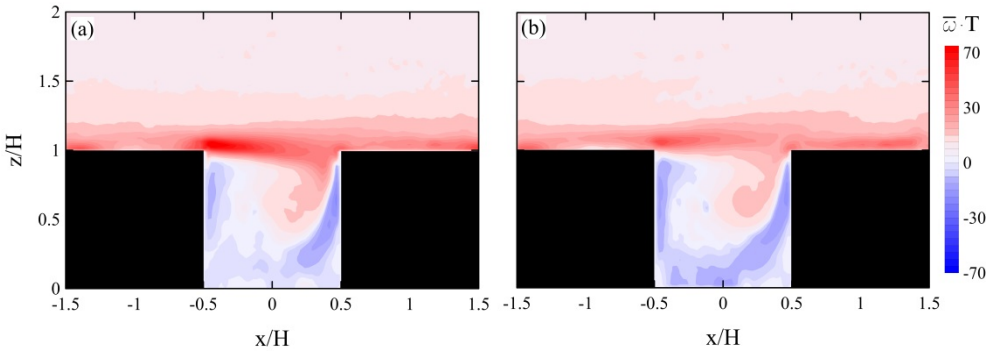

Fig. 9. Ensemble averages of vorticity fields during (a) sweeps and (b) ejections for AR=1.

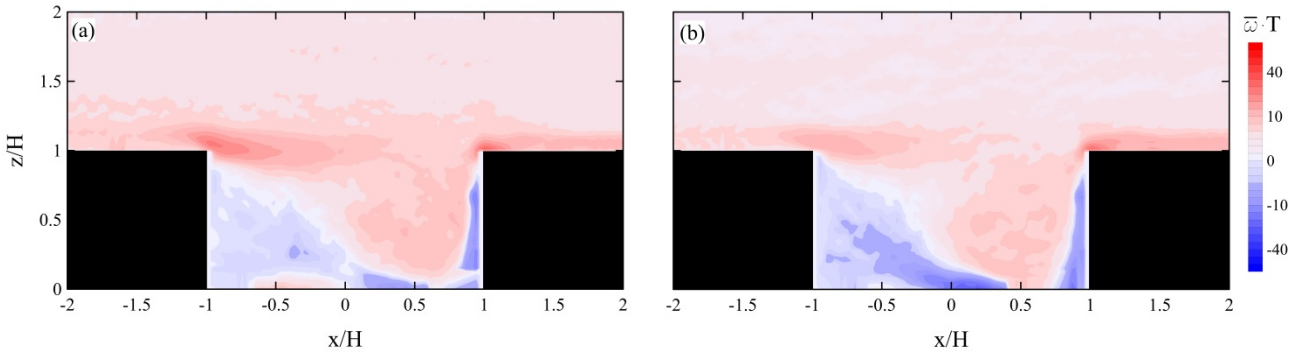

Fig. 10. As in Fig. 9, but for AR=2.

3.3. Quadrant analysis

Additional insights into the connection between shear layer flapping and turbulent fluxes of momentum and pollutants at the canyon top can be obtained using the so-called quadrant analysis, introduced by Willmarth (1975) and recently employed by Khan (2005), Nosek et al. (2016) and Ho and Liu (2017), among others. For a line source located at street level as considered in our experiments, events of sweep at the canyon top are associated with re-entrainment of polluted fluid (negative instantaneous vertical flux of tracer, $w'c'$) when $c' > 0$, while ejections permit venting of cleaner fluid when $c' < 0$, in both cases leading to a net transport of pollutants into the canyon ($w'c' < 0$). Events of positive $u'w'$ are generally termed outward ($w' > 0$) or inward ($w' < 0$) interactions (Figure 11).

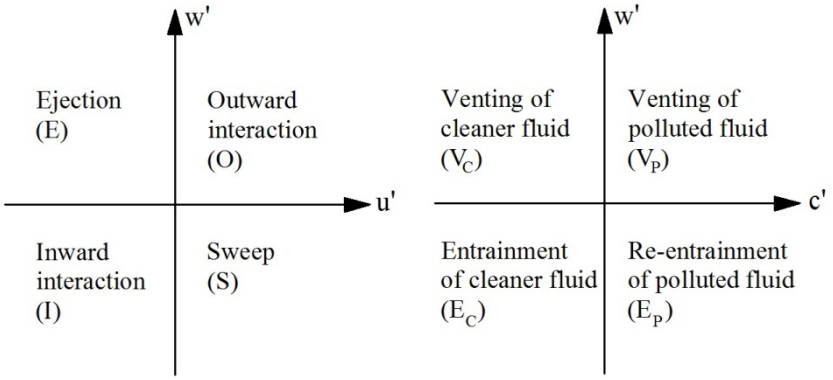

Fig. 11. Schematic of quadrant analysis.

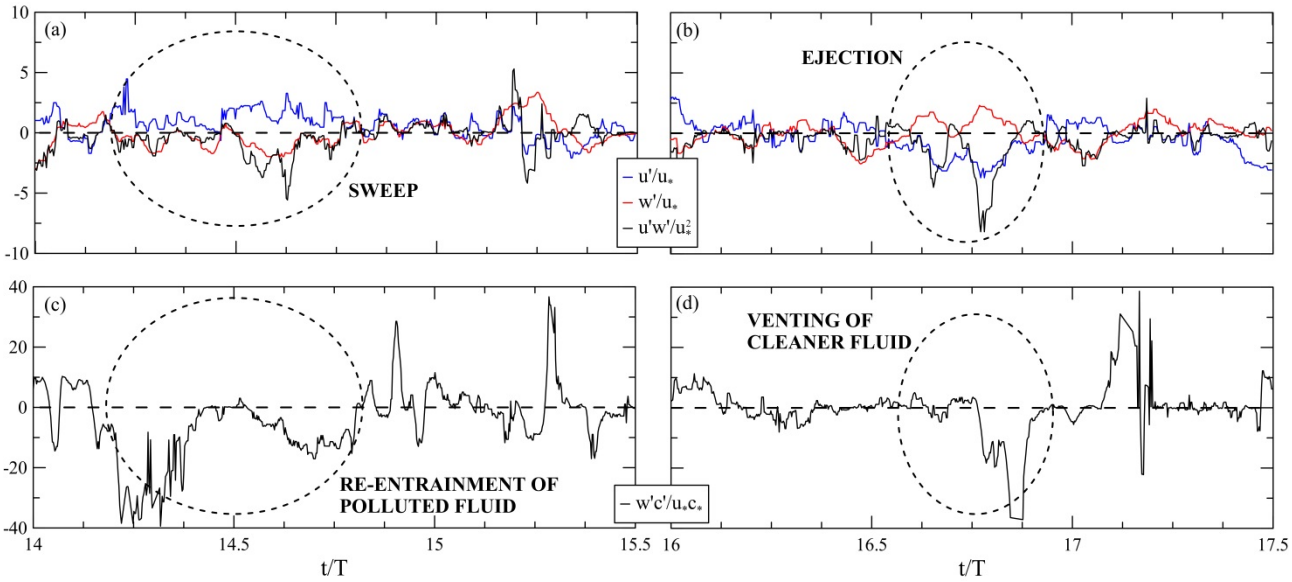

Fig. 12. (a) Time histories of the non-dimensional u', w' and $u'w'$, during an event of sweep and re-entrainment of polluted fluid ($c' > 0$) detected at z=H and x=0.25H for AR=1 and the corresponding eddy flux, $w'c'$ (c). Panels (b) and (d) are the counterparts of (a) and (c) during an event of ejection accompanied by venting of cleaner fluid ($c' < 0$).

Figure 12 shows examples of time histories of the fluctuating momentum flux of the non-dimensional velocity components and the fluctuating vertical tracer flux $w'c'$ (normalized by $u_* c_*$) measured at (x=-0.25H, z=H) for AR=1. Here, time t=0 corresponds to the start of the acquisition. The figure makes explicit the connection between momentum and pollutant fluxes in both sweeps and ejections. The ellipses encompass in panels (a) and (c) two sweep events ($u'w'<0$) associated with re-entrainment of polluted fluid ($w' < 0$ and $c' > 0$), while in panels (b) and (d) are encompassed two ejections associated with venting of cleaner fluid ($w' > 0$ and $c' < 0$).

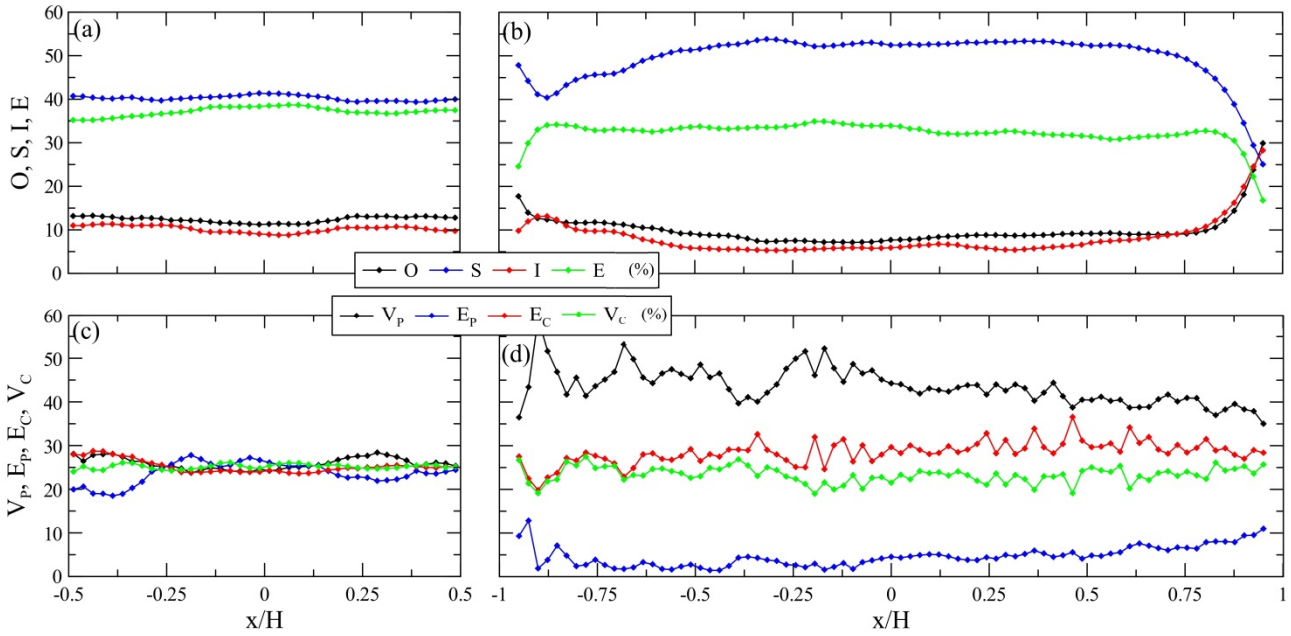

Fig. 13. Percentage of outward interaction (O), inward interaction (I), sweep (S) and ejection (E) calculated at z=H as a function of x/H for (a) AR=1 and (b) AR=2. Percentage of venting of polluted fluid (V_P), re-entrainment of polluted fluid (E_P), entrainment of cleaner fluid (E_C) and venting of cleaner fluid (V_C) calculated at z=H as a function of x/H for (c) AR=1 and (d) AR=2.

The contribution of both sweeps (S) and ejections (E) to $\overline{u'w'}$ is nearly 40% when AR=1 (Figure 13a). The remnant ≈20% is shared by inward (I) and outward (O) interactions that, as expected, play a secondary role in the vertical exchange of momentum (Leonardi et al., 2004). In terms of contributions to the average tracer flux, $\overline{w'c'}$, the weights of venting of polluted fluid (V_P), re-entrainment of polluted fluid (E_P), entrainment of clean fluid (E_C) and venting of clean fluid (V_C) are roughly the same and practically independent of x (Figure 13c). The only exception to this fact is the low E_P found near the upstream building where, not surprisingly, venting of polluted fluid and entrainment of cleaner fluid prevail. The four contributions to $\overline{u'w'}$ and $\overline{w'c'}$ for AR=2 are depicted in Figures 13b and 13d, respectively. Apart from the larger weight of sweep events, the most remarkable differences with AR=1 lie in the greater venting of polluted fluid ($\approx 40-50\%$) and the lower re-entrainment of polluted fluid ($\leq 10\%$) through the whole canyon top, almost negligible for x/H<0. Both these occurrences are the signatures of the far larger role played at the canyon top by the turbulent mixing, as it is four to five times higher than advection (see Sect. 3.6).

3.4. Pollutant and air exchange rates

The pollutant exchange rate, PCH, has proven to be a useful tool to quantify pollutants dilution in street canyons (Liu et al., 2005). It is obtained by integrating the instantaneous vertical pollutant flux at the canyon top:

$$\mathrm{PCH}(t) = \int_W w(t)c(t)dW. \quad (1)$$

PCH can be split into a positive (PCH_+) and negative (PCH_-) part based on the sign of w. The first term represents the removal of pollutants from the street canyon (w>0), while the latter quantifies pollutant re-entrainment into the cavity (w<0). Thus, PCH_+ reads as:

$$\mathrm{PCH}_+(t) = \int_W w_+(t)c(t)dW, \quad (2)$$

where w_+ refers to events with positive w. Similarly, PCH_- is associated with negative w.

Another suitable parameter introduced by Liu et al. (2005) is the air exchange rate, ACH, defined as the integral of the instantaneous vertical velocity measured at the canyon top:

$$\mathrm{ACH}(t) = \int_W w(t)dW. \quad (3)$$

Similarly to PCH, by splitting ACH into a positive, ACH_+,

$$\mathrm{ACH}_+(t) = \int_W w_+(t)dW \quad (4)$$

and negative (ACH_-) part it is possible to calculate the rate of fluid exchanged between the canyon and the overlying boundary layer. ACH_+ quantifies the fluid removal from the street canyon, while ACH_- represents the entry of external fluid into the canyon. The larger the ACH_+ the greater the canyon ventilation. Even if the air exchange through the canyon interface corresponds to the actual pollutant removal only under the assumption that the pollutant is well mixed within the canyon, ACH is often adopted when no information about the concentration field is available (Garau et al., 2018).

Figure 14 shows an example of the time histories of PCH/q, PCH_+/q, PCH_-/q and ACH_+/AT^{-1} for AR=1 (A=W·1 represents the area of the canyon top for unit width). As expected, PCH_+/q (blue line) is generally higher than PCH_-/q (red) and their time averages, $|\overline{\mathrm{PCH}_+}|/q$ and $|\overline{\mathrm{PCH}_-}|/q$, depend considerably on the AR values (Table 1). In particular, the ratio $|\overline{\mathrm{PCH}_+}|/|\overline{\mathrm{PCH}_-}|$ passes from ≈2.4 (for AR=1) to ≈10 (for AR=2), meaning that for the wake-interference regime pollutant re-entrainment plays a secondary, mainly because of the larger vertical mixing occurring above the cavity that facilitates the removal of the tracer from the canyon (see next subsection). Note that the

present results for AR=1 support the LES by Liu et al. (2005) and O'Neill et al. (2016).

Regarding air ventilation, Figure 14b shows that $\overline{ACH_+}/AT^{-1}$ is strictly related to PCH_+, as expected. The average values obtained for the two AR values confirm the idea that the greater the AR the larger the natural ventilation (see e.g. Badas et al., 2017).

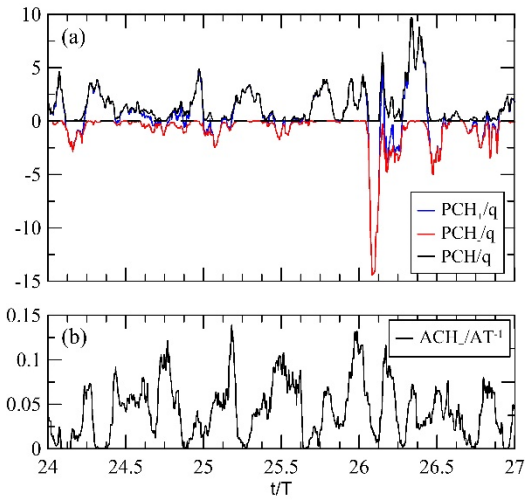

Fig. 14. (a) Time histories of the non-dimensional PCH/q, PCH_+/q and PCH_-/q calculated for AR=1. (b) As in (a), but for ACH_+/AT^{-1}. Details on the normalizations are reported in the text.

	$\overline{PCH_+}/q$	$\overline{PCH_-}/q$	$\overline{ACH_+}/AT^{-1}$
AR=1	1.716	-0.713	0.039
AR=2	1.08	-0.102	0.054

Table 1: Non-dimensional, time averaged pollutant and air exchange rates for AR=1 and 2.

3.5. Pollutant concentration statistics

Figures 15a and 15b show the mean non-dimensional concentration fields ($\overline{c}/c_*$) measured for AR=1 and 2, respectively. In the former case, the pollutant is initially advected from the source by the main vortex towards the leeward façade of the upstream building. Then it rises up towards the canyon top. The lower concentrations at the bottom corners of the cavity and at the top corner of the leeward building are caused by the small vortices seen in Figure 2. Once the pollutant leaves the canyon, the large streamwise velocity in the outer layer advects the pollutant downstream limiting the vertical extension of the plume, in agreement with other laboratory or numerical results (see e.g. Caton et al. (2003) and Li et al. (2016)).

The fate of the tracer released for AR=2 is somewhat different. In a large part of the downstream side of the cavity the concentration is much lower compared to that in the upstream side, giving rise to considerable spatial inhomogeneities of the mean concentration within the canyon, not present

for AR=1. The larger extent of the plume outside the canyon is a direct consequence of the stronger vertical mixing characterizing the wake-interference regime (see next subsection).

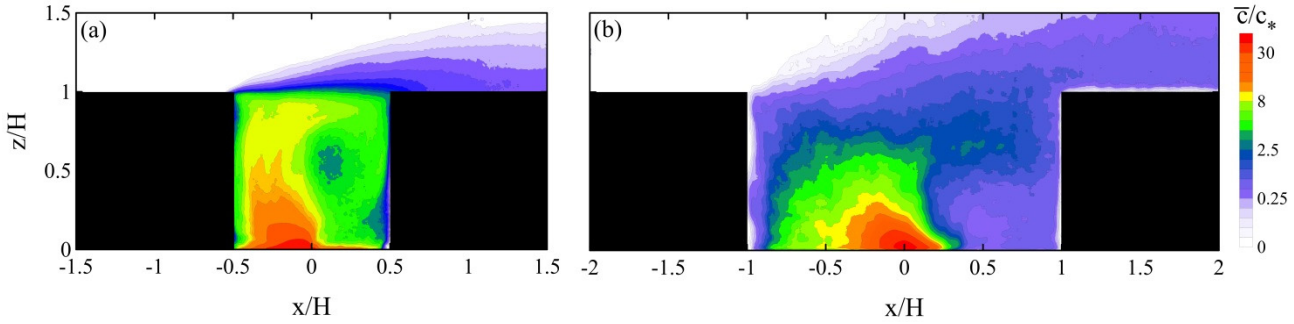

Fig. 15. Map of the non-dimensional mean concentration, $\overline{c}/c_*$, for (a) AR=1 and (b) AR=2.

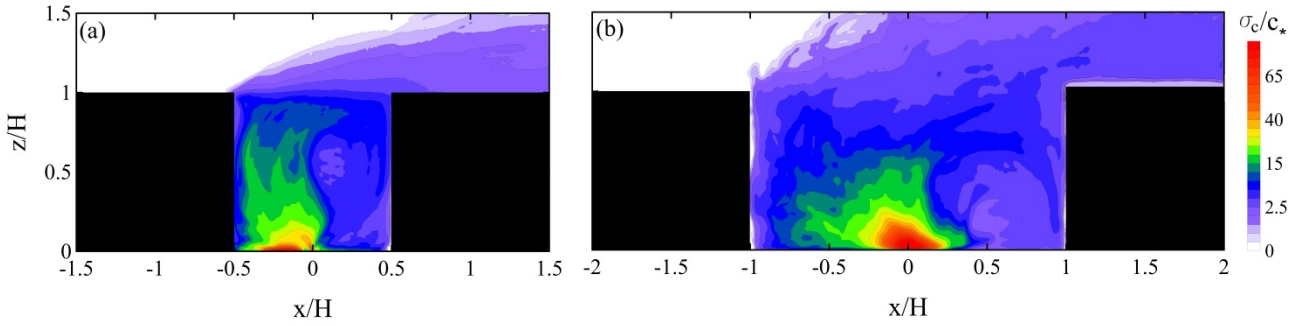

Fig. 16. As in Fig. 15, but for the non-dimensional standard deviation of concentration.

The higher values of the non-dimensional standard deviation of the concentration fluctuations (σ_c/c_*) roughly follow the plume propagating from the source (Figures 16), presumably caused by large concentration gradients combined with instantaneous plume patterns that rapidly vary in time. The region of relatively small σ_c/c_* in the initial part of the plume axis when AR=1 (Figure 16a) bears relation to the nature of the polluted plume, which is stable enough for that region to be persistently occupied by the plume core, thus determining small concentration fluctuations. Conversely, the area of high σ_c/c_* near the source for AR=2 is a result of the plume meandering from its initial stage. Outside that area, the lower gradients of $\overline{c}/c_*$ cause a decrease of σ_c/c_*, particularly close to the windward wall of the canyon. For both the AR values, $\sigma_c/c_* \approx 0$ at the corner of the windward building, in agreement with the LES by Liu et al. (2004). Worth noting also is that $\overline{c}/c_*$ and σ_c/c_* have the same order of magnitude, highlighting the importance of considering the standard deviation in quantitative concentration assessments conducted by means of appropriate numerical dispersion models, such as those based on the Lagrangian approach (Amicarelli et al., 2012; Amicarelli et al., 2017; Cassiani et al., 2013; Leuzzi et al., 2012; Marro et al., 2015).

The skewness factor of the concentration, $S_C = \overline{c'^3}/\sigma_c^3$, is a measure of the asymmetry of the

probability density function of c. Its knowledge can be of importance in phenomena such as explosions, accidental releases and impact of odor. Note that the skewness factor must be taken with a degree of caution, since the number of samples available in our analysis (25,000) might not be large enough to make the skewness contours adequately regular, especially above the canyon. S_C assumes only positive values in the field investigated (Figure 17), as expected for a quantity bounded below. Lower S_C take place where the plume is stably present or in areas of high concentration fluctuations. These situations occur almost everywhere in the canyon for AR=1 and within the upstream side of the canyon for AR=2. Near the source, S_C is lower for AR=2 because of the higher $\overline{c'^2}$ caused by the meandering of the polluted plume. On the other hand, S_C increases where sporadic peaks of concentration occur, e.g. in regions of low concentration. Such conditions are typical in the mixing area of the external flow, especially at the edge of the polluted plume, and in the region of entrainment of the external flow into the canyon, such as in the downstream half of the canyon for AR=2.

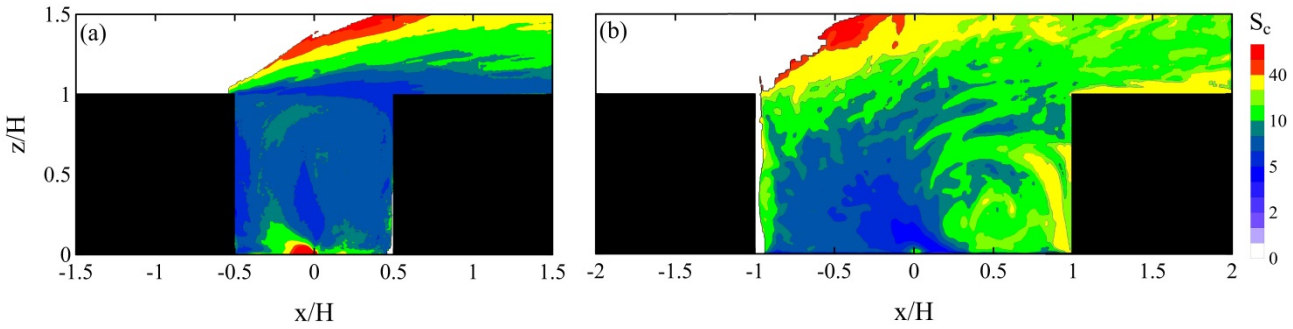

Fig. 17. Maps of the skewness factor of the concentration, S_C, for (a) AR=1 and (b) AR=2.

3.6. Advective and turbulent pollutant fluxes within the canopy

The turbulent tracer flux is a key parameter in transport and mixing of scalars as it appears in the balance equations of the mean and variance of the concentration of passive scalars dispersed in turbulent flows (see Batchelor (1959); Csanady (1967)). Unfortunately, turbulent fluxes are not known quantities and must be parameterized invoking closure rules based on empirical assumptions (Efthimiou et al., 2017). It is therefore of great importance to increase knowledge on pollutant fluxes in canopy flows, where strong inhomogeneities and anisotropies of the turbulence due to large shears make turbulence closures very problematic to achieve.

Here, the expected value of the pollutant vertical flux, $\overline{wc}$, is expressed as the sum of the mean (or advective) flux, $\overline{w}\overline{c}$, and the turbulent (or eddy) flux, $\overline{w'c'}$. The two latter quantities, normalized by u_*c_* and calculated for both the AR values, are presented in Figure 18.

For given AR, $\overline{w}\overline{c}/u_*c_*$ and $\overline{w'c'}/u_*c_*$ are qualitatively and quantitatively similar within the

canyon, while in the outer layer the vertical mean flux is negligible since $\overline{w} \approx 0$ for z>H. Owing to flow topology (see the streamlines in Figure 2), near the source both $\overline{w}\overline{c}/u_*c_*$ and $\overline{w'c'}/u_*c_*$ are minor for AR=1. An obvious feature we can discern from Figures 18 and 19 is that $\overline{w}\overline{c}/u_*c_*$ is positive (upward flux) in the upstream side of the canyon and negative (downward flux) in that downstream in accordance with $\overline{w}$. The large region of positive $\overline{w'c'}/u_*c_*$ above the canopy highlights the key role played by the turbulent fluxes in the spreading of pollutants in the outer flow. Note that the area of positive $\overline{w'c'}/u_*c_*$ for z>H exhibits a larger vertical extent for AR=2 (Figure 19b), confirming that the wake-interference regime is by far more effective than the skimming flow in the vertical mixing of pollutants emitted within the canopy.

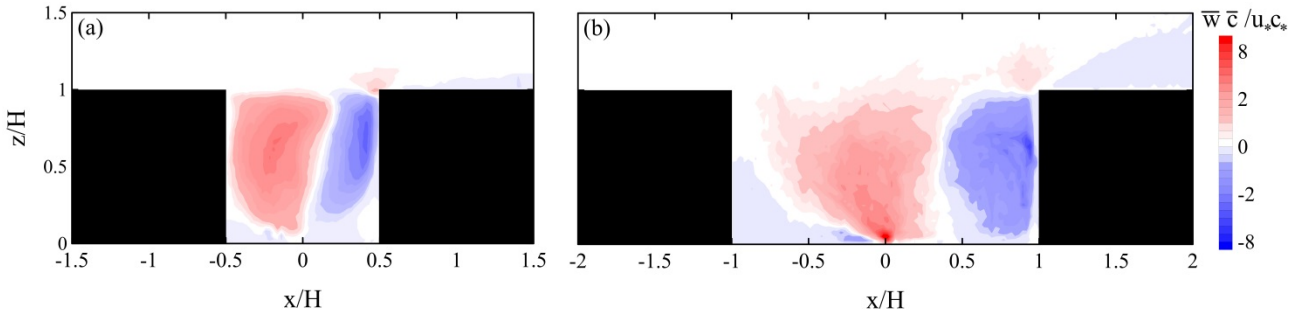

Fig. 18. Maps of $\overline{w}\overline{c}/u_*c_*$ for (a) AR=1 and (b) AR=2.

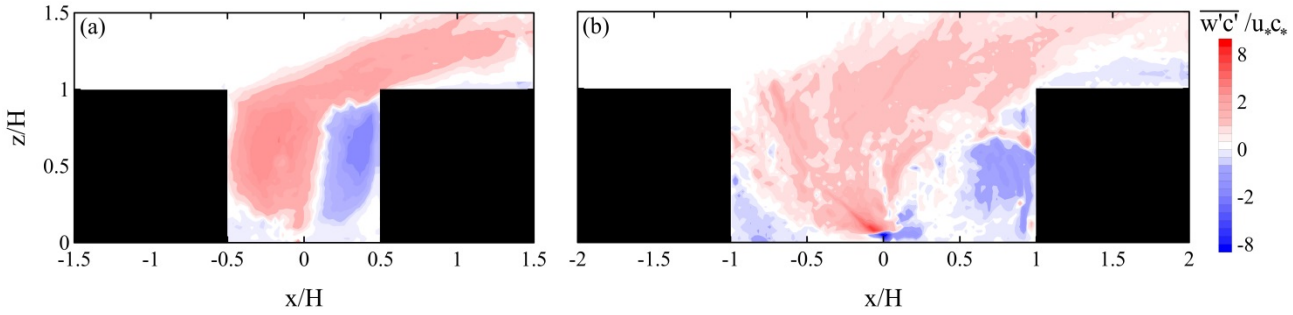

Fig. 19. Maps of $\overline{w'c'}/u_*c_*$ (a) for AR=1 and (b) AR=2.

To make the trends of the vertical fluxes at the canyon top clearer, their values calculated at z=H as a function of x/H are depicted in detail in Figure 20. For AR=1 (Figure 20a) the advective flux (green line) is positive for -0.5<x/H≲0.2, i.e. where $\overline{w} > 0$ (see Figure 2a). In contrast, the turbulent component $\overline{w'c'}/u_*c_*$ is positive over the entire interface (blue line) and is greater than $\overline{w}\overline{c}/u_*c_*$, in agreement with the LES by Michioka et al. (2011). A similar behavior was also found in three-dimensional canopies by Michioka et al. (2014) and Tomas et al. (2017). As a result, the total flux $\overline{w}\overline{c}/u_*c_*$ (red line) remains positive along the whole canyon top, with the exclusion of the area close to the windward building.

The trend of the vertical tracer fluxes along the canyon top changes when AR=2 (Figure 20b). As for the skimming flow, the turbulent flux is positive everywhere and shows a plateau for most of the canyon width. In contrast, the contribution from $\overline{wc}/u_*c_*$ to the total flux is almost negligible all over the interface and the negative zone near the windward building is now practically absent. In other terms, $\overline{wc}/u_*c_* \approx \overline{w'c'}/u_*c_*$ for AR=2, even though the peak of $\overline{wc}/u_*c_*$ is not far from that measured for AR=1.

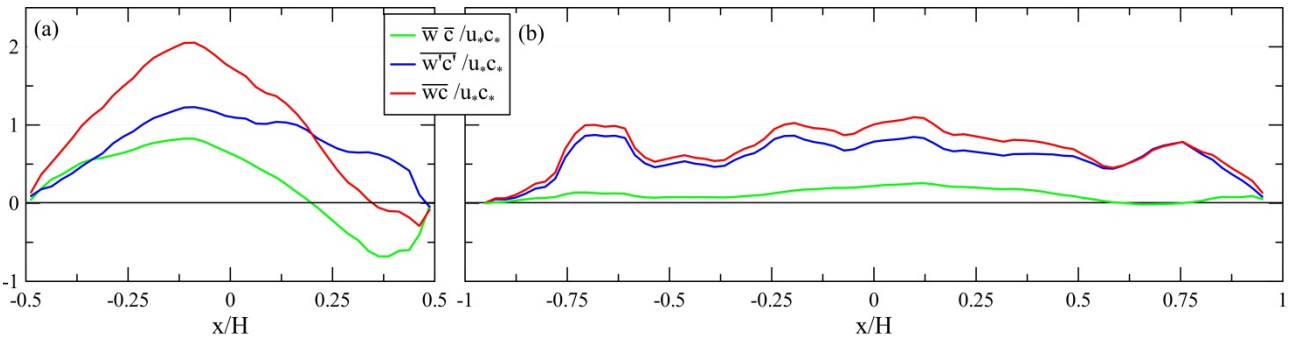

Fig. 20. Advective (green line), turbulent (blue line) and total (red line) non-dimensional tracer fluxes determined at the canyon top for (a) AR=1 and (b) AR=2.

According to Figure 20b, it is finally worth noting that, if one has the objective of studying urban-scale pollution in areas related to wake-interference regimes, the linear source at street level could be properly replaced by an area source, whose emission rate is homogeneously distributed over the canyon top. The same result does not apply for the skimming flow, where a clear modulation of the emission rate versus the streamwise direction appears.

4. Summary and conclusions

Pollutant fluxes in two-dimensional street canyons are analyzed through laboratory experiments conducted in a water channel simulating a neutral atmospheric boundary layer. Two geometrical arrangements with aspect ratios AR=1 and 2 are investigated using a line source in order to simulate emissions due to vehicular traffic. The experimental setup allows us to measure velocity and concentration fields simultaneously and permits the determination of pollutant fluxes with high spatial and temporal resolutions.

The results show the important influence of the aspect ratio, both on the statistical moments of the concentration and on the vertical momentum and pollutant fluxes. A strict connection is found between the shear layer location and the vorticity field at the canyon top for both the AR values, in agreement with Takimoto et al. (2011). Only for case AR=1 does the power spectral density of the vertical velocity component indicate that the shear layer flaps upwards and downwards at a

frequency comparable to that of the vortex shedding caused by the large velocity gradient present at the building top. The flapping of the shear layer controls ejection and sweep modes that, in turn, regulates venting and entrainment of both polluted and clean fluids at the canyon top. It is worth mentioning that the power spectra peaks also at a frequency corresponding to $T = H/u_*$, assumed here as the time scale of the flow and roughly equivalent to the time needed by a fluid particle to travel a complete recirculation within the canyon. The two frequencies correspond well to those visible in the power spectral density of the PCH. In other words, for the skimming flow regime the canyon breathes with two distinct and unrelated frequencies.

Another important disparity between the skimming flow and the wake-interferences regime lies in the different contributions to the total vertical concentration flux ($\overline{wc}$) from its mean ($\overline{w}\,\overline{c}$) and turbulent part ($\overline{w'c'}$). At the canyon top, while $\overline{w}\,\overline{c}$ and $\overline{w'c'}$ are comparable when AR=1, $\overline{w}\,\overline{c} \ll \overline{w'c'}$ for AR=2. This fact has also implications for the different pollutant exchange rates found for the two AR values and might also explain the reason why the pollutant re-entrainment is much lower than pollutant emission when AR=2.

Finally, the maps of the first three statistical moments of the pollutant concentrations show that the standard deviation is comparable to the mean all over the canyon. Besides, the non-negligible values of the skewness factor observed within the canyon, particularly close to the source, suggest that the knowledge of the first two statistical moments might be not sufficient to assess individual exposure in street canyons.

Acknowledgements

This work was funded by internal grant number C26A14BF3S.

References

Amicarelli, A., Salizzoni, P., Leuzzi, G., Monti, P., Soulhac, L., Cierco, F.-X., Leboeuf, F., 2012. Sensitivity analysis of a concentration fluctuation model to dissipation rate estimates. Int. J. Environ. Pollut. 48, n.1/2/3/4, 164-173. doi: 10.1504/IJEP.2012.049663.

Amicarelli, A., Leuzzi, G., Monti, P., Alessandrini, S., Ferrero, E., 2017. A stochastic Lagrangian micromixing model for the dispersion of reactive scalars in 578 turbulent flows: role of concentration fluctuations and improvements to the conserved scalar theory under non-homogeneous conditions. Environ. Fluid Mech. 17, 715-753. doi 10.1007/s10652-017-9516-1.

Badas, M.G., Ferrari, S., Garau, M., Querzoli, G., 2017. On the effect of gable roof on natural ventilation in two-dimensional urban canyons. J. Wind Eng. Ind. Aerodyn. 162, 24–34. http://dx.doi.org/10.1016/j.jweia.2017.01.006.

Baik, J.-J., Park, R.-S., Chun, H.-Y., Kim, J.-J., 2000. A laboratory model of urban street-canyon flows. J. Appl. Meteorol. 39, 1592–1600. doi: 10.1175/1520-0450(2000)039<1592:ALMOUS>2.0.CO;2.

Baik, J.-J., Kim, J.-J., 2002. On the escape of pollutants from urban street canyons. Atmos. Environ. 36, 527–536. doi: 10.1016/S1352-2310(01)00438-1.

Barlow, J.F., 2014. Progress in observing and modelling the urban boundary layer. Urban Clim. 10, 216–240. http://dx.doi.org/10.1016/j.uclim.2014.03.011.

Barlow, J.F., Harman, I.N., Belcher, S.E., 2004. Scalar fluxes from urban street canyons. Part I: laboratory simulation. Bound.-Layer Meteorol. 113, 369-385. doi: 10.1007/s10546-004-6204-8.

Batchelor, K., 1959. Small-scale variation of convected quantities like temperature in turbulent fluid, part 1: general discussion and the case of small conductivity. J. Fluid Mech., 5, 113–133. doi: 10.1017/S002211205900009X.

Buccolieri, R., Salizzoni, P., Soulhac, L., Garbero, V., Di Sabatino, S., 2015. The breathability of compact cities. Urban Clim. 13, 79-93.

Caton, F., Britter, R.E., Dalziel, S., 2003. Dispersion mechanisms in a street canyon. Atmos. Environ. 37, 693-703. doi: 10.1016/S1352-2310(02)00830-0.

Cassiani, M., 2013. The volumetric particle approach for concentration fluctuations and chemical reactions in Lagrangian particle and particle-grid models. Bound-Layer Meteorol. 146, 207–233.

Cenedese, A., Del Prete, Z., Miozzi, M., Querzoli, G., 2005. A laboratory investigation of the flow in the left ventricle of a human heart with prosthetic, tilting-disk valves. Exp. Fluids 39, 322–335. doi:10.1007/s00348-005-1006-4.

Csanady, G.T., 1967. Concentration fluctuations in turbulent diffusion. J. Atmos. Sci., 24, 21-28.

Dezső-Weidinger, G., Stitou, A., van Beeck, J., Riethmuller, M.L., 2003. Measurements of the turbulent mass flux with PTV in a street canyon. J. Wind Eng. Ind. Aerodyn. 91, 1117-1131. doi: 10.1016/S0167-6105(03)00054-0.

Di Bernardino, A., Monti, P., Leuzzi, G., Querzoli, G., 2015a. Water-channel study of flow and turbulence past a 2D array of obstacles. Bound.-Layer Meteorol. 155, 73-85. doi: 10.1007/s10546-014-9987-2.

Di Bernardino, A., Monti, P., Leuzzi, G., Querzoli, G., 2015b. On the effect of the aspect ratio on flow and turbulence over a two-dimensional street canyon. Int J Environ Pollut 58:27–38. doi: 10.1504/IJEP.2015.076581.

Di Bernardino, A., Monti, P., Leuzzi, G., Querzoli, G., 2017. Water-channel estimation of Eulerian and Lagrangian time scale of the turbulence in idealized two-dimensional urban canopies. Bound.-Layer Meteorol., In press. doi: 10.1007/s10546-017-0278-6.

Dutta, S., Muralidhar, K., Panigrahi, P.K., 2003. Influence of the orientation of a square cylinder on the wake properties. Exp. Fluids 34, 16–23. doi: 10.1007/s00348-002-0484-x.

Efthimiou, G.C., Andronopoulos, S., Bartzis, J.G., Berbekar, E., Harms, F., Leitl, B., 2017. CFD-RANS prediction of individual exposure from continuous release of hazardous airborne materials in complex urban environments. J. Turbul. 18, 115-137. doi: 10.1080/14685248.2016.1246736.

Fernando, H.J.S., 2010. Fluid dynamics of urban atmospheres in complex terrain. Annu. Rev. Fluid Mech. 42, 365-389.

Garau, M., Badas, M.G., Ferrari, S., Seoni, S., Querzoli, G., 2018. Turbulence and air exchange in two-dimensional urban street canyon between gable roof buildings. Bound.-Layer Meteorol. doi: 10.1007/s10546-017-0324-4.

Ho, Y.-K., Liu, C.-H., 2017. Street-level ventilation in hypothetical urban areas. Atmos. 8, 124. doi:10.3390/atmos8070124.

Hussain, M., Lee, B.M., 1980. An investigation of wind forces on three dimensional roughness elements in a simulated boundary layer flow. Report BS 56, Dept. of Building Science, University of Sheffield, 81.

Kastner-Klein, P., Plate, E.J., 1999. Wind-tunnel study of concentration fields in street canyons. Atmos. Environ. 33, 3973-3979. doi: 10.1016/S1352-2310(99)00139-9.

Khan, I.M., Simons, R.R., Grass, A.J., 2005. Upstream turbulence effect on pollution dispersion. Environ. Fluid Mech. 5, 393-413. doi: 10.1007/s10652-005-2932-7.

Kovar-Panskus, A., Louka, P., Sini, J.-F., Savory, E., Czech, M., Abdelqari, A., Mestayer, P.G., Toy, N., 2002. Influence of geometry on the mean flow within urban street canyons – A comparison of wind tunnel experiments and numerical simulations. Water, Air and Soil Pollution: Focus 2, 365-380. doi: 10.1023/A:1021308022939.

Krogstad, P.-Å., Andersson, H.I., Bakken, O.M., Ashrafian A., 2005. An experimental and numerical study of channel flow with rough walls. J. Fluid Mech. 530, 327-352. doi: 10.1017/S0022112005003824.

Leonardi, S., Orlandi, P., Djenidi, L., Antonia, R.A., 2004. Structure of turbulent channel flow with square bars on one wall. Int. J. Heat Fluid Flow 25, 384–392. doi:10.1016/j.ijheatfluidflow.2004.02.022.

Leuzzi, G., Amicarelli, A., Monti, P., Thomson, D.J., 2012. A 3D Lagrangian micromixing dispersion model LAGFLUM and its validation with a wind tunnel experiment. Atmos. Environ. 54, 117-126. doi: 10.1016/j.atmosenv.2012.02.054.

Li, X.-X., Britter, R.E., Koh, T.Y., Norford, L.K., Liu, C.-H., Entekhabi, D., Leung, D.Y.C., 2010. Large-eddy simulation of flow and pollutant transport in urban street canyons with ground heating. Bound.-Layer Meteorol. 137, 187-204. doi: 10.1007/s10546-010-9534-8.

Li, X.-X., Britter, R.E., Norford, L.K., 2016. Effect of stable stratification on dispersion within urban street canyons: a large-eddy simulation. Atmos. Environ. 144, 47-59 doi: 10.1016/j.atmosenv.2016.07.024.

Liu, C.-H., Barth, M.C., Leung, D.Y.C., 2004. Large-eddy simulation of flow and pollutant transport in street canyons of different building-height-to-street-width ratios. J. Appl. Meteorol. 43, 1410-1423. doi: 10.1175/JAM2143.1

Liu, C.-H., Leung, D.Y.C., Barth, M.C., 2005. On the prediction of air and pollutant exchange rates in street canyons of different aspect ratios using large-eddy simulation. Atmos. Environ. 39, 1567-1574. doi:10.1016/j.atmosenv.2004.08.036.

Louka, P., Belcher, S.E., Harrison, R.G. (2000) Coupling between air flow in streets and the well-developed boundary layer aloft. Atmos. Environ. 34, 2613-2621.

Marro, M., Nironi, C., Salizzoni, P., Soulhac, L., 2015. Dispersion of a passive scalar from a point source in a turbulent boundary layer. Part II: Analytical Modelling. Bound.-Layer Meteorol. 156, 447–469.

Michioka, T., Sato, A., Takimoto, H., Kanda, M., 2011. Large-eddy simulation for the mechanism of pollutant removal from a two-dimensional street canyon. Bound.-Layer Meteorol. 138, 195-213. doi: 10.1007/s10546-010-9556-2.

Michioka, T., Takimoto, H., Sato, A., 2014. Large-eddy simulation of pollutant removal from a three-dimensional street canyon. Bound.-Layer Meteorol 150(2), 259–275. doi:10.1007/s10546-013-9870-6

Monti, P., Querzoli, G., Cenedese, A., Piccinini, S., 2007. Mixing properties of a stably stratified parallel shear layer. Phys. Fluids, Vol. 19, Article number 085104 (1-9). doi: 10.1063/1.2756580.

Neophytou, M. K.-A., Markides, C.N., Fokaides, P.A., 2014. An experimental study of the flow through and over two dimensional rectangular roughness elements: deductions for urban boundary layer parameterizations and exchange processes. Phys. Fluids. 26, 086603. doi: 10.1063/1.4892979.

Nosek, S., Kukačka, L., Kellnerova, R., Jurčàkovà, K., Jaňour, Z., 2016. Ventilation processes in a three-dimensional street canyon. Bound.-Layer Meteorol. 159, 259-284. doi: 10.1007/s10546-016-0132-2.

Oke, T.R., 1987. Boundary-Layer Climates. Routledge, London, 435.

O'Neill, J.J., Cai, X.-M., Kinnersley, R., 2016. Stochastic backscatter modelling for the prediction of pollutant removal from an urban street canyon: a large-eddy simulation. Atmos. Environ. 142, 9-18. doi: 10.1016/j.atmosenv.2016.07.024.

Poggi, D., Katul, G.G., Cassiani, M., 2008. On the anomalous behavior of the Lagrangian structure function similarity constant inside dense canopies. Atmos. Environ. 42, 4212–4231. doi: 10.1016/j.atmosenv.2008.01.020.

Pournazeri, S., Schulte, N., Tan, S., Princevac, M., Venkatram, A., 2013. Dispersion of buoyant emissions from low level sources in urban areas: water channel modelling. Int. J. Environ. Pollut. 52, 119-140. doi: 10.1504/IJEP.2013.058460.

Salizzoni, P., Soulhac, L., Mejean, P. 2009a. Street canyon ventilation and atmospheric turbulence. Atmos. Environ. 43, 5056-5067. doi 10.1016/j.atmosenv.2009.06.045.

Salizzoni, P., Van Liefferinge, R., Soulhac, L., Mejean, P., Perkins, R.J. 2009b. Influence of wall roughness on the dispersion of a passive scalar in a turbulent boundary layer. Atmos. Environ. 43(3), 734-748. doi: 10.1016/j.atmosenv.2008.07.057.

Salizzoni, P., Marro, M., Soulhac, L., Grosjean, N., Perkins, R.J., 2011. Turbulent transfer between street canyons and the overlying atmospheric boundary layer. Bound.-Layer Meteorol. 141, 393-414. doi:10.1007/s10546-011-9641-1.

Snyder, W.H., 1972. Similarity criteria for the application of fluid models to the study of air pollution meteorology. Bound.-Layer Meteorol. 3, 113–134. doi: 10.1007/BF00769111.

Takimoto, H., Sato, A., Barlow, J.F., Moriwaki, R., Inagaki, A., Onomura, S., Kanda, M., 2011. Particle image velocimetry measurements of turbulent flow within outdoor and indoor urban scale models and flushing motions in urban canopy layers. Bound.-Layer Meteorol. 140, 295-314. doi: 10.1007/s10546-011-9612-6.

Tomas, J.M., Eisma, H.E.,·Pourquie, M.J.B.M., Elsinga, G. E., Jonker, H. J. J., Westerweel, J., 2017. Pollutant Dispersion in Boundary Layers Exposed to Rural-to-Urban Transitions: Varying the Spanwise Length Scale of the Roughness. Bound.-Layer Meteorol. 163, 225–251. doi: 10.1007/s10546-016-0226-x.

Uehara, K., Wakamatsu, S., Ooka, R. 2003. Studies on critical Reynolds number indices for wind-tunnel experiments on flow within urban areas. Bound.-Layer Meteorol. 107, 353–370. doi: 10.1023/A:1022162807729.

Vinçont, J.-Y., Simoëns, S., Ayrault, M., Wallace, J.M., 2000. Passive scalar dispersion in a turbulent boundary layer from a line source at the wall and downstream of an obstacle. J. Fluid Mech., 424, 127-167. doi: 10.1017/S0022112000001865.

Willmarth, W.W., 1975. Structure of turbulence in boundary layers. Arch. Appl. Mech., 15, 159–254. doi: 10.1016/S0065-2156(08)70057-7.

Zajic, D., Fernando, H.J.S., Brown, M.B, Kim, J.-J., Baik, J.-J., 2003. Flow and turbulence in simulated city canyons; measurements and computations. Fifth International Conference on Urban Climate, 1-5- September, 2003. Lodz, Poland, 4 p.